Boundary-Layer Meteorol (2007) 124:315–333
DOI 10.1007/s10546-007-9177-6

ORIGINAL PAPER

SHEBA flux–profile relationships in the stable atmospheric boundary layer

Andrey A. Grachev · Edgar L Andreas · Christopher W. Fairall · Peter S. Guest · P. Ola G. Persson

Received: 2 March 2006 / Accepted: 5 March 2007 / Published online: 17 April 2007

Abstract Measurements of atmospheric turbulence made during the Surface Heat Budget of the Arctic Ocean Experiment (SHEBA) are used to examine the profile stability functions of momentum, φ_m, and sensible heat, φ_h, in the stably stratified boundary layer over the Arctic pack ice. Turbulent fluxes and mean meteorological data that cover different surface conditions and a wide range of stability conditions were continuously measured and reported hourly at five levels on a 20-m main tower for 11 months. The comprehensive dataset collected during SHEBA allows studying φ_m and φ_h in detail and includes ample data for the very stable case. New parameterizations for $\varphi_m(\zeta)$ and $\varphi_h(\zeta)$ in stable conditions are proposed to describe the SHEBA data; these cover the entire range of the stability parameter $\zeta = z/L$ from neutral to very stable conditions, where L is the Obukhov length and z is the measurement height. In the limit of very strong stability, φ_m follows a $\zeta^{1/3}$ dependence, whereas φ_h initially increases with increasing ζ, reaches a maximum at $\zeta \approx 10$, and then tends to

A. A. Grachev · P. O. G. Persson
Cooperative Institute for Research in Environmental Sciences,
University of Colorado, Boulder, CO, USA

A. A. Grachev (✉) · C. W. Fairall · P. O. G. Persson
NOAA Earth System Research Laboratory,
Boulder, CO, USA
e-mail: Andrey.Grachev@noaa.gov

E. L Andreas
U.S. Army Cold Regions Research and Engineering Laboratory,
Hanover, NH, USA

Present address:
E. L Andreas
NorthWest Research Associates, Inc. (Bellevue Division),
25 Eagle Ridge, Lebanon, NH 03766-1900, USA

P. S. Guest
Naval Postgraduate School,
Monterey, CA, USA

level off with increasing ζ. The effects of self-correlation, which occur in plots of φ_m and φ_h versus ζ, are reduced by using an independent bin-averaging method instead of conventional averaging.

Keywords Arctic Ocean · Flux–profile relationships · Monin–Obukhov similarity theory · SHEBA Experiment · Stable boundary layer

1 Introduction

Understanding the characteristics of turbulent transport to and from the Earth's surface is a central problem of atmospheric boundary-layer research. Traditionally, turbulent fluxes are derived from vertical wind speed and temperature profiles (flux–profile relationships), and the importance of the flux–profile relationships for climate modelling, weather forecasting, environmental impact studies, and many other applications has long been recognized.

Well-known predictions of the flux–profile relationships are based on the theory suggested over 50 years ago by Monin and Obukhov (1954). There is a long history of testing Monin–Obukhov predictions including profile functions (see, for example, the surveys in Monin and Yaglom 1971; Dyer 1974; Yaglom 1977; Dyer and Bradley 1982; Högström 1988; Sorbjan 1989; Garratt 1992; Andreas 2002). Perhaps the Businger–Dyer profile functions are the most widely and routinely used flux–profile relationships in the unstable case (Dyer and Hicks 1970; Paulson 1970; Businger et al. 1971). Considerably fewer studies exist that cover very stable conditions. In fact, a simple linear interpolation (log-linear law) proposed at the end of the 1960s by Zilitinkevich and Chalikov (1968) and Webb (1970) that provides blending between neutral and very stable cases is still widely used. Subsequently, several alternative empirical forms have been proposed for more strongly stable conditions (Holtslag and De Bruin 1988; Beljaars and Holtslag 1991).

Investigating the turbulence structure in the stable boundary layer (SBL) is of great practical importance, especially for air pollution studies (Mahrt 1999), because the SBL develops almost every night over land surfaces. Progress in understanding SBL has been restrained because the SBL is often continually evolving and the turbulence is generally weak. In addition, several scaling regimes are identified in the SBL that are associated with different physical mechanisms (e.g., Holtslag and Nieuwstadt 1986; Smedman 1988; Mahrt et al. 1998; Grachev et al. 2005). Furthermore, several different definitions are possible for the SBL height (e.g., Zilitinkevich and Mironov 1996; Zilitinkevich and Baklanov 2002). Examining the SBL is also complicated by slope flows, low-level jets, meandering motions, influence of gravity waves, and other phenomena (e.g., Mahrt 1999). Some insight into the SBL structure has been gained through several experimental studies (e.g., Forrer and Rotach 1997; Mahrt et al. 1998; Howell and Sun 1999; Pahlow et al. 2001; Yagüe et al. 2001; Mahrt and Vickers 2002; Klipp and Mahrt 2004; Cheng and Brutsaert 2005; Hartogensis and De Bruin 2005; Yagüe et al. 2006).

In this paper, we use the extensive dataset from the Surface Heat Budget of the Arctic Ocean Experiment (SHEBA) to study the profile stability functions and to derive new parameterizations for them in stable conditions. The SHEBA measurement program, which took place from October 1997 to October 1998, was the most ambitious scientific effort ever attempted in the Arctic (Andreas et al. 1999; Persson

et al. 2002). Turbulent fluxes and mean meteorological data were continuously measured at five levels on a 20-m main tower, supported by comprehensive atmospheric, oceanographic, and ice/snow data (Uttal et al. 2002). The 11 months of measurements during SHEBA cover a wide range of stability conditions, from weakly unstable to very stable stratification, and allow us to study the physical nature of the SBL, including the very stable cases, in detail.

Limited observations still remain a problem for SBL model validation. However, the turbulence data collected over the Arctic pack ice during SHEBA offer several advantages for studying the structure of the SBL compared to traditional nocturnal boundary-layer measurements at mid-latitudes. The theme that the polar regions are ideal meteorological "laboratories" is a recurrent one in the literature (cf. Andreas et al. 2000). At high latitudes, especially during the polar night, the long-lived SBL can reach very stable and quasi-stationary states. Besides, the Arctic pack ice is a rather uniform, flat surface without large-scale slopes, and as a result, our SHEBA data are not contaminated by drainage (katabatic) or strong advective flows. The almost unlimited and extremely uniform fetch provides an opportunity to isolate many physical processes, with conditions that are nearly ideal for studying flux–profile relationships under stable conditions.

2 Formal background

Monin–Obukhov similarity theory (MOST) has provided a framework for describing turbulence in the stratified atmospheric surface layer. According to MOST (Monin and Obukhov 1954), properly scaled dimensionless statistics of the turbulence are universal functions of a stability parameter, $\zeta = z/L$, defined as the ratio of the reference height z and the Obukhov length scale (Obukhov 1946, 1971),

$$L = -\frac{u_*^3\,\theta_v}{\kappa g < w'\theta_v' >}, \tag{1}$$

where u_* is the friction velocity, θ_v is the virtual potential temperature, κ is the von Kármán constant, and g is the acceleration due to gravity. It should be noted that Eq. 1 is based on the *surface* momentum flux, $\tau_o = \rho u_*^2 = -\rho < u'w' >$, and the *surface* buoyancy flux, $b_o = (g/\theta_v) < w'\theta_v' >$ (ρ is air density, u and w are the longitudinal and vertical velocity components, respectively, $(')$ denotes fluctuations about the mean value, and $< \quad >$ is a time/space averaging operator).

Specifically, the non-dimensional vertical gradients of mean wind speed (U) and potential temperature (θ) in the MOST are assumed to be

$$\frac{\kappa z}{u_*}\frac{\mathrm{d}U}{\mathrm{d}z} = \varphi_m(\zeta), \tag{2a}$$

$$\frac{\kappa z}{\theta_*}\frac{\mathrm{d}\theta}{\mathrm{d}z} = \varphi_h(\zeta), \tag{2b}$$

where $\theta_* = - < w'\theta' > /u_*$ is the temperature scale based on the *surface* potential temperature flux, and $\varphi_m(\zeta)$ and $\varphi_h(\zeta)$ are non-dimensional universal functions ('stability profile functions'). In this study, the traditional value of $\kappa = 0.4$ is used for both wind speed and temperature profiles.

The exact forms of the universal functions (2) are not predicted by MOST and must be determined from measurements. However, in the neutral case ($\zeta \equiv 0$) these functions equal unity by definition, and MOST does predict the asymptotic behaviour of these functions under very stable ($\zeta >> 1$) and extremely unstable stratification (free convection, $\zeta << -1$).

In the very stable case ($\zeta >> 1$), MOST predicts that specific quantities become independent of z; that is, z is no longer a primary scaling variable (Obukhov 1946; Monin and Obukhov 1954). This result is because stable stratification inhibits vertical motion, and the turbulence no longer communicates significantly with the surface (Monin and Yaglom 1971; Holtslag and Nieuwstadt 1986; Mahrt 1999). Wyngaard and Coté (1972) and Wyngaard (1973) apparently first referred to this limit as 'z-less stratification'. The z-less concept requires that z cancels in Eq. 2a,b, which leads to (e.g., Garratt 1992)

$$\varphi_m(\zeta) = \beta_m \zeta, \tag{3a}$$

$$\varphi_h(\zeta) = \beta_h \zeta, \tag{3b}$$

where β_m and β_h are numerical coefficients. It is worth noting that the original MOST predicts that only β_m in Eq. 3a is a constant, whereas β_h in Eq. 3b may be a function of ζ (see the discussion in Monin and Yaglom 1971, Sect. 7.3). Since MOST does not specify β_h, a constant value was subsequently accepted for β_h (e.g., Garratt 1992).

For near-neutral conditions and moderate ranges of ζ, observations suggest (e.g. Zilitinkevich and Chalikov 1968; Webb 1970)

$$\varphi_m(\zeta) = 1 + \beta_m \zeta, \tag{4a}$$

$$\varphi_h(\zeta) = 1 + \beta_h \zeta, \tag{4b}$$

with these linear equations fitting the available experimental data well for $\zeta < 1$ (Businger et al. 1971; Dyer 1974; Yaglom 1977; Dyer and Bradley 1982; Högström 1988; King 1990). Measurements suggest $\beta_m \approx \beta_h \approx 5$ (Sorbjan 1989; Garratt 1992). Note that Eq. 4a, b would be the linear approximation for fairly small values of ζ if Eq. 2a, b were expanded in a power series to yield (3a) and (3b) in the limit $\zeta \to \infty$.

During 1960–1980, the idea arose that Eq. 4 also applied for stronger stability, including the limit of very stable stratification (e.g., Garratt 1992). However, during the past decade, this view has been seriously challenged. Forrer and Rotach (1997), Howell and Sun (1999), Yagüe et al. (2001, 2006), Klipp and Mahrt (2004), and Cheng and Brutsaert (2005) reported that the stability functions increase more slowly with increasing stability than predicted by Eqs. 3 or 4; and moreover, one (φ_h) or both functions become approximately constant in very stable conditions. Based on an analysis of standard deviations covering almost five orders of magnitude in ζ, Pahlow et al. (2001) found that they do not follow the z-less predictions; their results, therefore, suggest that the concept of z-less stratification generally does not hold. In Sect. 4, we consider in detail the behaviour of the φ_m and φ_h functions in the limit of very strong stability based on the SHEBA data.

The wind speed and temperature profiles in the general, non-neutral case are derived by integrating Eq. 2a, b (Panofsky 1963). Traditionally, these integral forms of the flux–gradient relations are expressed with the neutral and diabatic contributions separated:

$$U(z) = \frac{u_*}{\kappa}\left[\ln\frac{z}{z_o} - \Psi_m\left(\frac{z}{L}\right) + \Psi_m\left(\frac{z_o}{L}\right)\right], \tag{5a}$$

$$\theta(z) - \theta_{\mathrm{o}} = \frac{\theta_*}{\kappa}\left[\ln\frac{z}{z_{\mathrm{ot}}} - \Psi_h\left(\frac{z}{L}\right) + \Psi_h\left(\frac{z_{\mathrm{ot}}}{L}\right)\right]. \tag{5b}$$

Here, θ_{o} is the surface potential temperature, z_{o} is the aerodynamic roughness length, and z_{ot} is the temperature roughness length. The functions Ψ_m in Eq. 5a and Ψ_h in Eq. 5b obey

$$\Psi_m(\zeta) = \int_0^{\zeta} \frac{1-\varphi_m(\xi)}{\xi}\mathrm{d}\xi, \tag{6a}$$

$$\Psi_h(\zeta) = \int_0^{\zeta} \frac{1-\varphi_h(\xi)}{\xi}\mathrm{d}\xi. \tag{6b}$$

The purpose of our study is to revisit the empirical functional forms of φ_m, φ_h, Ψ_m, and Ψ_h for stable conditions based on the SHEBA data.

3 The SHEBA dataset

The SHEBA ice camp was centred around the Canadian icebreaker *Des Groseilliers*, which was frozen into the Arctic ice pack and drifted in the Beaufort Gyre from early October 1997 until early October 1998. During this period, the icebreaker drifted more than 2800 km in the Beaufort and Chukchi seas, with coordinates varying from approximately 74° N and 144° W to 81° N and 166° W.

Turbulent fluxes and mean meteorological data were continuously measured at five levels, nominally 2.2, 3.2, 5.1, 8.9, and 18.2 m (or 14 m during most of the winter), on the 20-m main SHEBA tower. Each level on the main tower had a Väisälä HMP-235 temperature and relative humidity probe and identical Applied Technologies, Inc. (ATI) three-axis sonic anemometer/thermometers (K-probe) that sampled at 10 Hz. An Ophir fast infrared hygrometer was mounted at about 8 m above the snow or ice surface (just below level 4). Except for rare periods, instruments ran almost continuously during 11 months. Turbulent covariance values and appropriate variances at each level are based on 1-h averaging and derived through the frequency integration of the cospectra and spectra (for other details, see Persson et al. (2002)).

Several data-quality indicators based on objective and subjective methods have been applied to the original flux data. Flux data have been edited for unfavourable relative wind direction for which the tower and the other camp structures were upwind of the sonic anemometers, noting that the wind blew from disturbed areas only about 10% of the time. Most of the station structures and the *Des Groseilliers* itself were located within these sectors. The undisturbed sector at SHEBA had a natural sea ice surface for many hundreds of kilometres with almost unlimited and uniform fetch. Some other quality-control criteria are based on validity limits for the horizontal (σ_u and σ_v) and vertical (σ_w) velocity standard deviations: $\sigma_u < 2\,\mathrm{m\,s^{-1}}$, $\sigma_v < 2\,\mathrm{m\,s^{-1}}$, and $\sigma_w < 0.7\,\mathrm{m\,s^{-1}}$. The main SHEBA tower was instrumented for over 8000 h, with over 6000 h of that period yielding useful data.

A number of corrections traditionally are applied for eddy-covariance measurements, many of which result from limitations in the instruments or non-ideal boundary-layer conditions (i.e., advection, non-simple terrain). As mentioned earlier the Arctic pack ice is a rather uniform, flat surface without large-scale slopes and heterogeneity. For this reason, coordinate system rotation to account for the slope of the

terrain (Wilczak et al. 2001) and corrections for advection (Paw U et al. 2000) are not required in our case.

Note that while Kaimal and Finnigan (1994, p. 219) suggested that ATI sonic anemometers not be used below a height of 4 m for adequate flux estimates, Kristensen and Fitzjarrald (1984) pointed out that adequate flux measurements can be made at heights of several (4–5) times the anemometer path separation. With a path length between transducers of 0.15 m, the ATI anemometer can be used for accurate variance measurements as low as 0.6 m. Andreas et al. (2006) showed that, because of path separation, flux measurements made by ATI sonic anemometers should be performed at least 1.7 m above the surface to avoid significant flux loss in SHEBA data. This result is a little stronger than Kristensen and Fitzjarrald (1984) estimations above. All measurements at SHEBA, including level 1 (2.2 m), satisfied these criteria.

In our analysis no corrections on the turbulent fluxes for loss of spectral energy (e.g., Moore 1986; Horst 2000; Massman 2000) were performed. Errors caused by inadequate frequency response and sensor separations depend on wind speed, boundary-layer stability, the height of the sensors above the ground, and the type of instruments deployed. However, they are insignificant for the sensible heat and momentum fluxes in our case (Andreas et al. 2006, pp. 123–124). Note also that according to Forrer and Rotach (1997), the corrections for the sensible heat flux and for friction velocity, which were measured with one single instrument (i.e., anemometer/thermometer), are typically less than 10% for $\zeta = 0.1$. These corrections on the latent heat flux (basically due to the sensor separation) may be 40% (their Fig. 4), but the moisture correction term in ζ and in sonic temperature is usually small for Arctic conditions (Grachev et al. 2005, p. 205).

Comprehensive analysis of different flux frequency response correction methods (Moore 1986: Horst 2000; Massman 2000; and their variations) was performed by Clement (2004). According to the Clement (2004) study, different methods for stable conditions give an average net correction between 1% and 2% for sensible heat flux (Ibid. Fig. 7.9) and less than 2% for the momentum flux (Ibid. Fig. 7.13). However, Clement (2004) also found that, for low wind speeds, flux loss for sensible heat flux can be up to 30% (Ibid. Fig. 7.11). Because low wind speeds are usually associated with strong stability, these corrections to the sensible heat flux at $\zeta = 100$ can be as large as 5–30% for different methods (Ibid. Fig. 7.12). The same conclusions can be applied to the momentum flux; large corrections are associated with low wind speeds (Ibid. Fig. 7.15) and very stable stratification (Ibid. Fig. 7.16). To avoid possible significant flux loss, wind speeds $\leq 1\,\mathrm{m\,s^{-1}}$ have been excluded from our data. According to the Clement (2004) study, flux loss corrections for stable conditions are less than 5–10% (for the different methods tested) under this restriction (Ibid. Figs. 7.11 and 7.15).

The 'slow' temperature and humidity probes provided air temperature and relative-humidity measurements at five levels and were used to evaluate the vertical temperature gradient in Eq. 2. The mean wind speed was derived from the sonic anemometers. Rotation is needed to place the measured wind components in a streamwise coordinate system. We used the most common method, which is a double rotation of the anemometer coordinate system, to compute the longitudinal, lateral, and vertical velocity components.

The vertical gradients in Eq. 2 were obtained by fitting the following second-order polynomial through the 1-h profiles:

$$x(z) = p_1(\ln z)^2 + p_2 \ln z + p_3, \tag{7}$$

where $x(z)$ represents either the wind speed, U, or the potential temperature, θ, at measurement level z, and p_1, p_2, and p_3 are the polynomial coefficients. The gradients and, thus, φ_m and φ_h were determined by taking the derivative of Eq. 7 with respect to z and evaluating it at each of the five tower levels.

Other details of the SHEBA program, the ice camp, deployed instruments, data processing, accuracy, calibration, and archived data files can be found in Andreas et al. (1999, 2002, 2003, 2006), Persson et al. (2002), Uttal et al. (2002), and Grachev et al. (2002, 2005).

4 Profile functions observed during SHEBA

The comprehensive SHEBA dataset allows us to study in detail the behaviour of φ_m and φ_h and other relevant turbulent features under stable conditions and sheds light on their behaviour in the limit of very strong stability. In this section, we consider different aspects of how φ_m and φ_h depend on the bulk Richardson number and ζ, with special emphasis on spurious self-correlation.

Traditionally, the non-dimensional gradients φ_m and φ_h are plotted versus ζ. However, a troubling feature of this analysis is that the same variables (primarily u_*) appear in both the definitions of φ_m and φ_h and in ζ, see Eqs. 1 and 2. For this reason, analyses for φ_m and φ_h versus ζ may have built-in correlation (or self-correlation) that can lead to erroneous results (e.g., Hicks 1978; Mahrt et al. 1998; Andreas and Hicks 2002; Klipp and Mahrt 2004). For example, decreasing u_* increases ζ and φ_m and decreases φ_h. As a result, dependencies of φ_m and φ_h on ζ could be due to self-correlation, also referred to as artificial, fictitious, or spurious correlation.

To obtain more reliable and independent estimates of the stability profile functions (2) over a wide range of stable conditions, we plot φ_m and φ_h versus the bulk Richardson number,

$$\mathrm{Ri}_B = -\left(\frac{gz}{\theta_v}\right)\frac{(\Delta\theta + 0.61\theta_v \Delta q)}{U^2}, \tag{8}$$

where $\Delta\theta$ and Δq are differences in the potential temperature and the specific humidity, respectively, between the surface and reference level z. Figures 1 and 2 show such plots for φ_m and φ_h for both surface and local scaling. Functions $\varphi_{m\,(1)}$ and $\varphi_{h\,(1)}$ in Figs. 1a and 2a are based on the fluxes measured at level 1 ('surface fluxes'), whereas $\varphi_{m\,(n)}$ and $\varphi_{h\,(n)}$ in Figs. 1b and 2b are based on the local fluxes at height z_n ($n = 1-5$) rather than on the surface values (Nieuwstadt 1984; Holtslag and Nieuwstadt 1986; Sorbjan 1989). Wind-speed and temperature gradients in these functions, $\varphi_{m\,(1)}$, $\varphi_{m\,(n)}$, $\varphi_{h\,(1)}$, and $\varphi_{h\,(n)}$, are referred to level n. The bin-averaged points in Figs. 1 and 2, based on the averaging of the individual one-hour data for Ri_B, φ_m, and φ_h are indicated by different symbols for each measurement level.

The individual 1-h-averaged data based on the median fluxes and other medians (heights, temperatures, etc.) for the five levels are also shown in Figs. 1 and 2 as background x-symbols. These points give an estimate of the available data at all levels and the typical scatter of the data. The median fluxes are computed from the median cospectra (i.e., at each frequency a median is computed from the values from the heights where data are available). The vertical dashed lines correspond to a critical Richardson number. According to the SHEBA data (Grachev et al. 2002, 2005), a

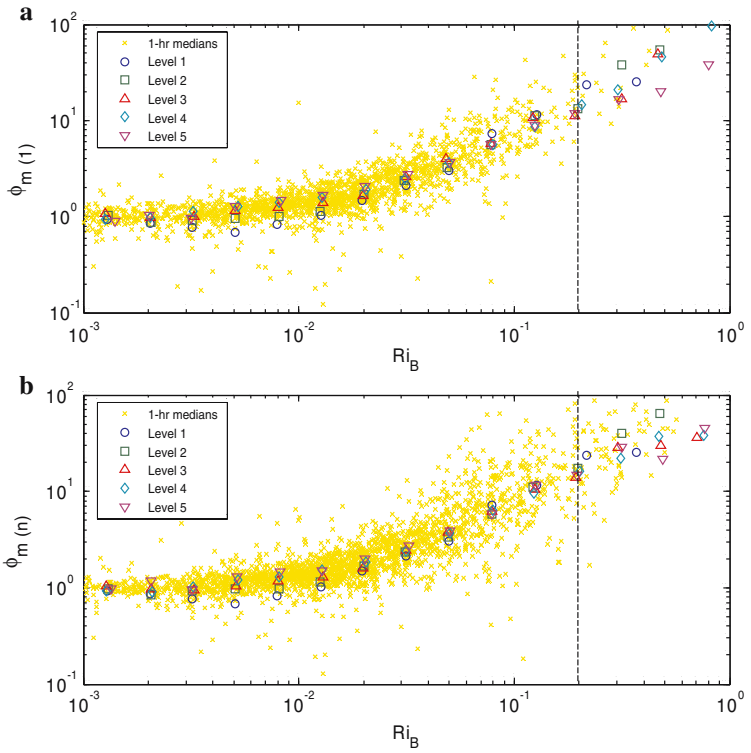

Fig. 1 Plots of the bin-averaged non-dimensional velocity gradient, φ_m, against the bulk Richardson number, Ri_B, for levels 1–5 during the 11 months of measurements. The functions φ_m in panel **a** are based on the fluxes measured at level 1 ('surface fluxes'), whereas φ_m in panel **b** are based on the local fluxes ($n = 1 - 5$). The vertical dashed lines correspond to $\mathrm{Ri}_B = 0.2$. Individual 1-h averaged data based on the median fluxes for the five levels are shown as the background x-symbols

bulk Richardson number, Eq. 8, of about 0.2 may be considered as the critical value; that is, $\mathrm{Ri}_{B\,cr} \approx 0.2$.

Figures 1 and 2 show that the averaged stability functions have different behaviours in the very stable regime. According to Fig. 1, φ_m increases with increasing stability up to the critical Richardson number. At the same time, φ_h, shown in Fig. 2, initially increases with increasing Ri_B and then almost levels off at $\mathrm{Ri}_B \approx 0.1$ (Fig. 2a). Figure 1 shows that there is no visible difference in plots for φ_m if we use surface (Fig. 1a) or local scaling (Fig. 1b). However, according to Fig. 2, using surface scaling instead of local scaling leads to less scatter between different observation levels for φ_h (cf. Grachev et al. 2005).

Although plots of φ_m and φ_h versus Ri_B are useful for qualitative analyses of these functions, theoretical formulations and parameterizations assume a functional dependence of φ_m and φ_h on ζ. Before plotting the φ_m and φ_h functions versus ζ, it is necessary to determine a range of ζ that corresponds to values $\mathrm{Ri}_B < 0.2$. Figure 3 shows ζ plotted against Ri_B for different levels. Although the dependence of ζ on Ri_B is not a universal function an average value of $\zeta = O(10)$ may be associated with $\mathrm{Ri}_B \approx 0.2$. However, some individual points in Fig. 3 for which $\mathrm{Ri}_B < 0.2$ reach values

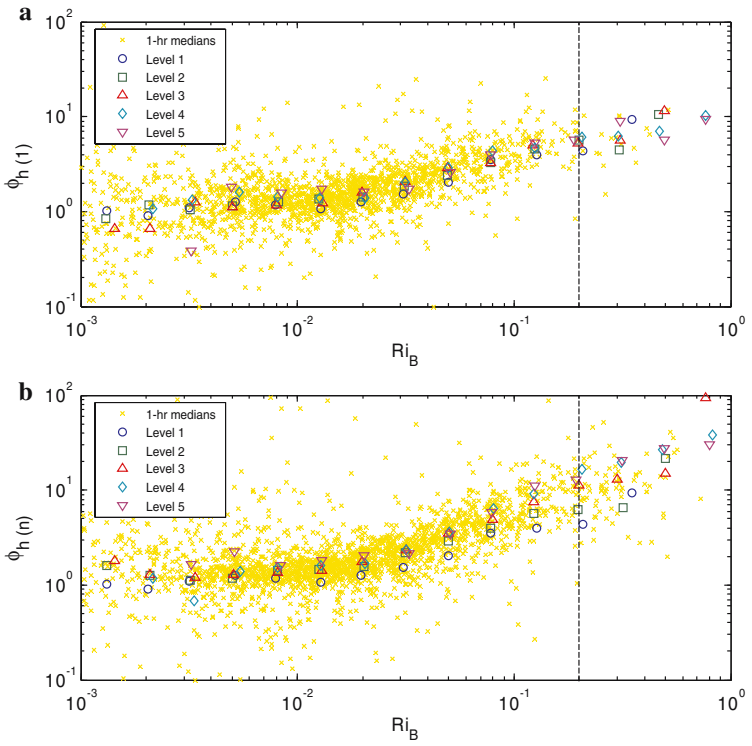

Fig. 2 Same as Fig. 1 but for the non-dimensional temperature gradient, φ_h. Data with a temperature difference between the air (at median level) and the snow surface less than 0.5°C have been omitted to avoid the large uncertainty in determining the sensible heat flux

up to $\zeta \approx 100$. Therefore, it makes sense to plot the φ_m and φ_h functions versus ζ in the range $\zeta \leq 100$.

Plots of the non-dimensional gradients of the wind speed and temperature versus the stability parameter for the five tower levels during the 11 months of the SHEBA measurements are presented in Figs. 4 and 5. These functions are plotted in the log-log coordinates for z_n/L_1 and $z_n/L_n \leq 100$ (cf. Fig. 3).

As discussed above, plots of $\varphi_m(\zeta)$ and $\varphi_h(\zeta)$ versus ζ are affected by self-correlation. For this reason, the plain bin-averaging used in Figs. 1 and 2 would be affected if used in Figs. 4 and 5, too. To reduce or even to avoid the averaging problems associated with self-correlation, in Figs. 4 and 5 we used an independent bin-averaging method instead of conventional averaging in Figs. 1 and 2. First, we sorted the data for the value of one parameter (sorting parameter) into bins. We averaged z_n/L_1 (Figs. 4a, 5a) and z_n/L_n (Figs. 4b, 5b) in bins of width $10^{0.2}$. We then computed mean and median values of $< u'w' >$, $< w'T' >$, $\mathrm{d}U/\mathrm{d}z$, $\mathrm{d}\theta/\mathrm{d}z$, and other relevant variables for each bin. Based on these averaged values, we finally computed stability parameters (1) and φ functions (2) for the surface and local scaling. Furthermore, stability parameters plotted on the horizontal axis are based on the mean values, and the φ functions plotted on the vertical axis are based on the medians.

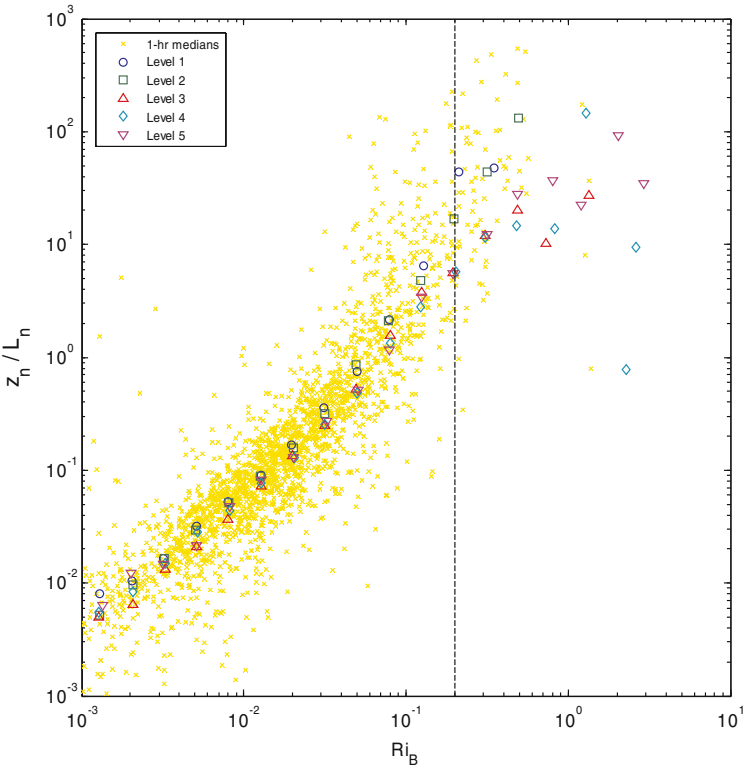

Fig. 3 Dependence of the local stability parameter, z_n/L_n, on the bulk Richardson number, Ri_B. The vertical dashed line corresponds to the critical Richardson number, $\mathrm{Ri}_B = 0.2$. Symbols are the same as in Fig. 1

According to the SHEBA data presented in Fig. 4, the stability function φ_m increases more slowly than predicted by the linear Eq. 4a and follows a $\zeta^{1/3}$ dependence in the very stable regime (cf. Grachev et al. 2005, their Fig. 14; Yagüe et al. 2006, their Figs. 3, 4). At the same time, the stability function φ_h initially increases with increasing ζ, reaches a maximum at $\zeta \approx 10$, and tends to level off at large ζ (Fig. 5). This behaviour means that the temperature profile becomes logarithmic again under very stable conditions. According to Figs. 4 and 5, using surface scaling instead of local scaling leads to less scatter between different observation levels for both φ_m and φ_h, especially for strong stability (cf. Figs. 1, 2). However, both stability functions φ_m and φ_h expressed with local scaling (Figs. 4b, 5b) show slightly better fits with the Beljaars–Holtslag relationships than those expressed with surface scaling (Figs. 4a, 5a). Cheng and Brutsaert's (2005) parameterization, based on the CASES-99 data ($\zeta \leq 5$), assumes that both functions level off for strongly stable conditions. The SHEBA data agree well with the Cheng and Brutsaert relationship for φ_m (their Eq. 22) up to $\zeta \leq 3$ but do not support their asymptotic behaviour for this function (Fig. 4a). In contrast, the Cheng and Brutsaert relationship for φ_h (their Eq. 24) describes well the asymptotic behaviour of the SHEBA data but overestimates the data in the range $0.1 \leq \zeta \leq 5$ (Fig. 5a). In addition, the variation of the turbulent Prandtl number based on the Cheng and Brutsaert parameterization with stability

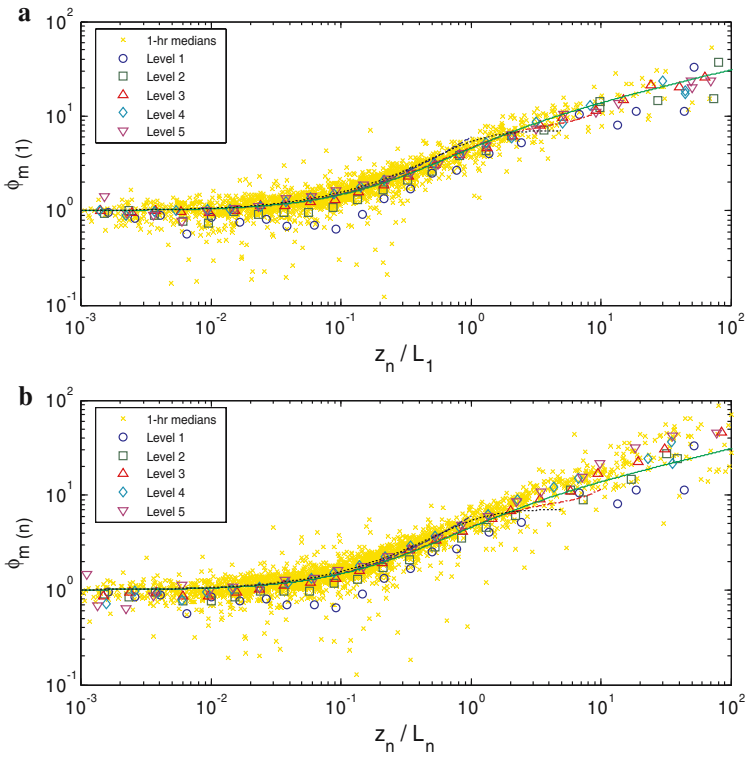

Fig. 4 Plots of the bin-averaged non-dimensional velocity gradient, φ_m, in log–log coordinates against (**a**) the surface stability parameter, z_n/L_1, and (**b**) the local stability parameter, z_n/L_n, for five levels ($n = 1 - 5$) during the 11 months of measurements. The dashed line represents $\varphi_m = \varphi_h = 1 + \beta\zeta$ with $\beta = 5(\zeta < 1)$, the dashed-dotted line is based on the Beljaars and Holtslag (1991) formula ($\zeta < 10$), and the dotted line is the Cheng and Brutsaert (2005) parameterization ($\zeta < 5$). The solid line is $\varphi_{m\,\mathrm{SHEBA}}$, Eq. 9a. Function $\varphi_{m\,(1)}$ and L_1 (upper panel) are based on the 'surface fluxes', whereas $\varphi_{m\,(n)}$ and L_n (bottom panel) are based on the 'local fluxes'. The wind speed gradient in both functions, $\varphi_{m\,(1)}$ and $\varphi_{m\,(n)}$, is based on the measurements at level n. Individual 1-h averaged data based on the median fluxes for the five levels are shown as the background x-symbols

is not monotonic in contrast to the monotonic decrease in the SHEBA data (see Sect. 5). Note, that Yagüe et al. (2006) using SABLES-98 data also reported that φ_m and φ_h tend to level off for $\zeta > 1 - 2$, whereas Hartogensis and De Bruin (2005) found good agreement between CASES-99 data and the Beljaars and Holtslag (1991) relationships.

Grachev et al. (2005) noted that the observed dependence $\varphi_m \propto \zeta^{1/3}$ (Fig. 4a) can be formally derived from Eq. 2a if one assumes that $\mathrm{d}U/\mathrm{d}z$ is independent of u_* for $\zeta >> 1$, implying that the stress (or friction velocity, u_*) is no longer a primary scaling parameter in the equation for $\mathrm{d}U/\mathrm{d}z$; they termed this regime frictionless (or 'u_*-less') scaling by analogy with the concept of 'z-less' scaling. The dramatic reduction of the surface stress is responsible for the main features of the atmospheric boundary layer in the limit of very strong stability. First, this regime is associated with the strong influence of the Earth's rotation. Frictional effects become negligible and the influence of the Coriolis effect becomes significant. Observed wind speeds show features of the

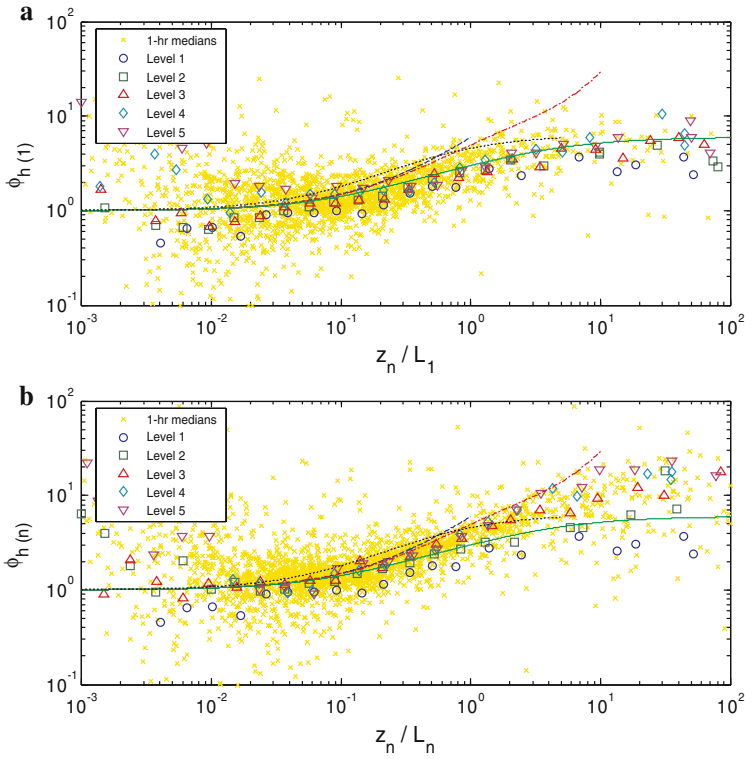

Fig. 5 Same as Fig. 4 but for the non-dimensional temperature gradient, φ_h. Data with a temperature difference between the air (at median level) and the snow surface less than 0.5°C have been omitted to avoid the large uncertainty in determining the sensible heat flux

Ekman spiral even near the surface (Grachev et al. 2002, 2005). Second, the stress falls off faster with increasing stability than the heat flux (Grachev et al. 2002, 2003, 2005), and the stress ceases to be a relevant scaling parameter in the relationship for $\mathrm{d}U/\mathrm{d}z$ in the limit of very strong stability. However, it is unlikely that the 'u_*-less' concept can be applied to φ_h. This approach would lead to the dependence $\varphi_h \propto \zeta^{-1/3}$, but according to Fig. 5, φ_h tends to be a constant in the range $10 < \zeta < 100$. According to Grachev et al. (2005, Fig. 15), some decrease in φ_h is observed for $\zeta > 100$ (cf. Yagüe et al. 2006, their Figs. 7, 8), but this is associated with the supercritical regime and may result largely from self-correlation.

According to Figs. 4 and 5, the bin averages for both φ_m and φ_h at levels 3–5 collapse better to a single curve over a wide range of z/L than the data obtained at levels 1 and 2. The data for these two lower levels are systematically lower than the data at the three higher levels. This bias is more pronounced in the wind speed profile for weakly and moderately stable conditions ($0.01 < z/L < 1$) and a possible reason of this phenomenon is discussed below. For this reason new parameterizations for φ_m and φ_h (Sect. 5) are based on the data collected at levels 3–5.

In Fig. 6, we examine the departure of the wind speed at levels 1–5 from the logarithmic profile for near-neutral conditions ($z_n/L_n < 0.1$ and $U > 4\,\mathrm{m\,s^{-1}}$). According to Fig. 6, the wind speeds at levels 4 and 5 are more or less described by the logarithmic

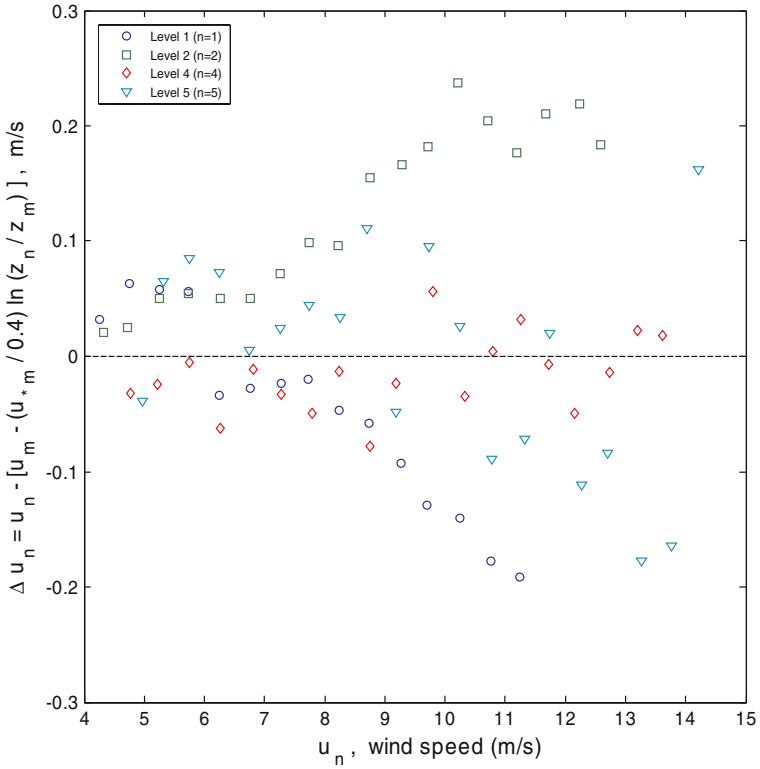

Fig. 6 Deviation of the wind speed at levels 1–5 from the logarithmic law for near-neutral conditions ($z_n/L_n < 0.1$ and $U > 4\,\mathrm{m\,s^{-1}}$). In the calculations, $u_{*\,m}$ is the median friction velocity, while u_m and z_m refer to level 3. For simplicity, stability corrections are not used here

law. For $U > 7-8\,\mathrm{m\,s^{-1}}$, the wind speed at level 1 is systematically lower and at level 2 is systematically higher than predicted by the logarithmic law. Although the deviation is small (about $0.2\,\mathrm{m\,s^{-1}}$ at $U \approx 10\,\mathrm{m\,s^{-1}}$, i.e. 2%) this behaviour may lead to the pronounced bias in the wind-speed gradients. The observed departure from the logarithmic profile in Fig. 6 may represent a real physical process, e.g. the logarithmic profile along the lower part of the tower is not in steady-state for winds higher than $7–8\,\mathrm{m\,s^{-1}}$, a surface flux footprint effect, or a blowing snow effect. It may also be a measurement artefact associated with this wind speed range. However as mentioned earlier, this effect has no impact on our parameterizations derived in this range from the measurements at levels 3–5 only.

5 The SHEBA stability functions

Traditional linear (Webb 1970; Businger et al. 1971; Dyer 1974) and Beljaars and Holtslag (1991) relationships fit most atmospheric datasets well for small and moderate values ζ when $\zeta > 0$. However, they overestimate existing data for large ζ. In essence, for large ζ, the linear relationships (4) and the Beljaars–Holtslag equation for φ_m are based on the z-less stratification concept. Although the Cheng and Brutsaert

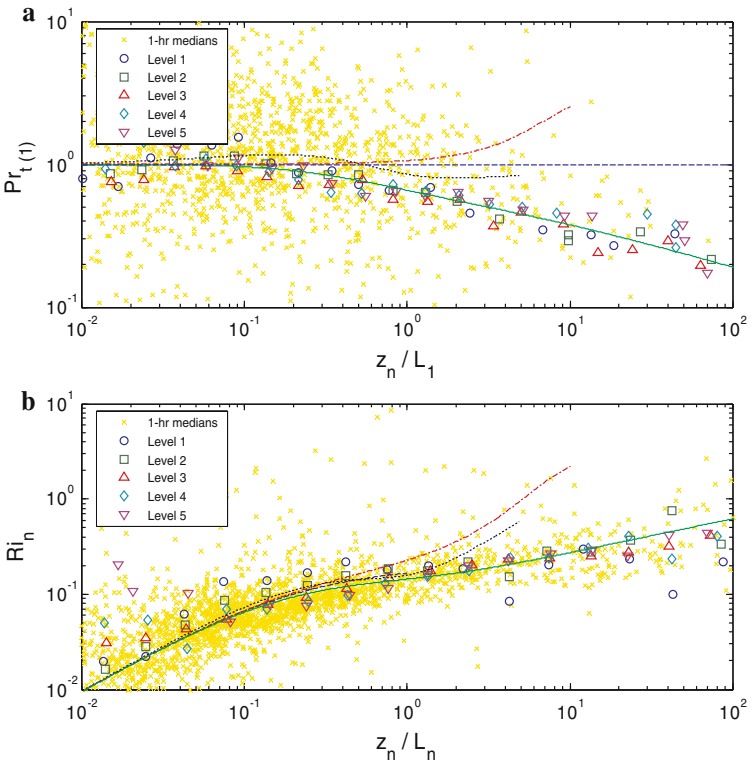

Fig. 7 Plots of the bin-averaged turbulent Prandtl number, Pr_t, (**a**) and gradient Richardson number, Ri, (**b**) versus ζ. Notation for symbols and lines is the same as in Figs. 4 and 5

(2005) parameterization is based on the recent CASES-99 data and covers a range up to $\zeta \approx 5$, there is some discrepancy between their results and the SHEBA data, as discussed above. In this section, we propose new functional forms for φ_m and φ_h in stable conditions based on the SHEBA data.

The functional forms for $\varphi_m(\zeta)$ and $\varphi_h(\zeta)$ proposed here are based on the following principals: (i) the functions should have proper behaviour, i.e., $\varphi_m(\zeta) \to 1 + \beta_m\zeta$ and $\varphi_h(\zeta) \to 1 + \beta_h\zeta$ for small ζ, and $\varphi_m \propto \zeta^{1/3}$ and $\varphi_h \to$ constant for $\zeta \to \infty$; (ii) $\varphi_m(\zeta)$ and $\varphi_h(\zeta)$ should fit the SHEBA data reasonably well for the entire range of $\zeta > 0$; and (iii) $\varphi_m(\zeta)$ and $\varphi_h(\zeta)$ should be analytically integrable, that is, $\Psi_m(\zeta)$ and $\Psi_h(\zeta)$ should be analytical functions (see Eq. 6).

A number of functions that satisfy the above criteria have been tested. Note that some interpolations suggested earlier for free convection and modified for $\zeta > 0$ can be applied here for $\varphi_m(\zeta)$. Power law interpolations have the general form suggested by Wilson (2001), $\varphi_m(\zeta) = (1 + \gamma_m\,\zeta^{k_m})^{n_m}$ and $\varphi_h(\zeta) = (1 + \gamma_h\,\zeta^{k_h})^{n_h}$. The exponent combination used by Carl et al. (1973) is $(k_m\ ,\ n_m\ ) = (k_h\ ,\ n_h\ ) = (1, -1/3)$. Kansas-type relationships are associated with the combination $(k_m\ ,\ n_m\ ) = (1, -1/4)$ and $(k_h\ ,\ n_h\ ) = (1, -1/2)$ for unstable conditions and $(k_m\ ,\ n_m\ ) = (k_h\ ,\ n_h\ ) = (1, 1)$ for stable stratification (see Eq. 4), and Wilson (2001) suggested an alternative function $(k_m\ ,\ n_m\ ) = (k_h\ ,\ n_h\ ) = (2/3, -1/2)$ for $\zeta < 0$. These functions, however, have the

undesirable property that the derivatives of both φ_m and φ_h approach infinity as ζ approaches zero.

The concept of 'u_*-less' stratification requires that $k_m n_m = 1/3$. The following combinations have been tested on the SHEBA dataset (k_m , n_m) = (1/3, 1), (1, 1/3), (2/3, 1/2), (1/2, 2/3). Our analysis demonstrated that all these cases lead to unsatisfactory agreement with the data. Thus, a simple interpolation with one coefficient (γ_m) cannot describe the SHEBA data. Functional forms suggested by Kader and Yaglom (1990, their Eq. 3.6) for $\zeta < 0$ with several calibration coefficients could also be adopted for the stable case, but these equations are not analytically integrable.

We thus suggest the following functional forms of $\varphi_m(\zeta)$ and $\varphi_h(\zeta)$ based on the SHEBA data ('the SHEBA profile functions'):

$$\varphi_{m\ \mathrm{SHEBA}} = 1 + \frac{a_m \zeta (1+\zeta)^{1/3}}{1 + b_m \zeta} \equiv 1 + \frac{6.5\zeta(1+\zeta)^{1/3}}{1.3 + \zeta}, \tag{9a}$$

$$\varphi_{h\ \mathrm{SHEBA}} = 1 + \frac{a_h \zeta + b_h \zeta^2}{1 + c_h \zeta + \zeta^2} \equiv 1 + \frac{5\zeta + 5\zeta^2}{1 + 3\zeta + \zeta^2}, \tag{9b}$$

where $a_m \equiv \beta_m = 5$, $b_m = a_m/6.5$, $a_h \equiv \beta_h = 5$, $b_h = 5$, and $c_h = 3$. Coefficients a_m and a_h are determined from the asymptotic behaviour of $\varphi_m(\zeta)$ and $\varphi_h(\zeta)$ for small ζ (see Eq. 4); the ratio a_m/b_m and coefficient b_h are derived from the asymptotic behaviour of these functions at $\zeta \to \infty$. Note that $\varphi_m \to (a_m/b_m)\zeta^{1/3} = 6.5\zeta^{1/3}$ and $\varphi_h \to 1 + b_h = 6$ as $\zeta \to \infty$. Coefficient c_h is derived by fitting the data for moderate ranges of ζ. The proposed parameterizations for the stability functions φ_m and φ_h, Eq. 9, are plotted versus the stability parameter in Figs. 4 and 5 (solid lines). As discussed above, the surface scaling is superior to the local scaling.

Parameterizations (9) have also been used to study the behaviour of the turbulent Prandtl number and the gradient Richardson number (Fig. 7) (cf. Andreas 2002). Note that the difference between φ_m and φ_h is best demonstrated by plots of the turbulent Prandtl number defined by

$$\mathrm{Pr}_t = \frac{k_m}{k_h} = \frac{< u'w' >\ \mathrm{d}\theta/\mathrm{d}z}{< w'\theta' > \mathrm{d}U/\mathrm{d}z} \equiv \frac{\varphi_h}{\varphi_m}, \tag{10}$$

where $k_m = -\frac{<u'w'>}{\mathrm{d}U/\mathrm{d}z}$ is the turbulent viscosity, and $k_h = -\frac{<w'\theta'>}{\mathrm{d}\theta/\mathrm{d}z}$ is the turbulent thermal diffusivity. The turbulent Prandtl number (10) describes the difference in turbulent transfer between momentum and sensible heat; turbulent momentum transfer is more efficient than turbulent heat transfer when $\mathrm{Pr}_t > 1$ and vice versa.

The gradient Richardson number, Ri, is defined by

$$\mathrm{Ri} = \left(\frac{g}{\theta_v}\right) \frac{\mathrm{d}\theta_v/\mathrm{d}z}{(\mathrm{d}U/\mathrm{d}z)^2} = \frac{\zeta \varphi_h}{\varphi_m^2}. \tag{11}$$

Note that Pr_t and Ri depend more sensitively on the parameterizations for $\varphi_m(\zeta)$ and $\varphi_h(\zeta)$ because both parameters are combinations of φ_m and φ_h. The flux Richardson number, in contrast, contains only one function, $\mathrm{Rf} = \zeta/\varphi_m$. According to Eq. 10, Pr_t may be defined for local and for surface scaling as we have done for $\varphi_m(\zeta)$ and $\varphi_h(\zeta)$. The relationship (11) for Ri contains no fluxes, and therefore Ri is defined only locally.

According to Fig. 7a, on average, Pr_t tends to be less than 1 with increasing stability by virtue of the asymmetric behaviour of the φ_m and φ_h functions (Figs. 1, 2, 4 and 5).

Note also that according to Grachev et al. (2002, 2003, 2005), a small but still significant heat flux (several W m^{-2}) and negligibly small stress characterize the very stable regime. This asymmetric flux decay causes k_m to decrease faster than k_h and therefore leads Pr_t to decrease (see Eq. 10). Our result $\mathrm{Pr}_t < 1$ is consistent with Howell and Sun (1999) but disagrees with the measurements of Kondo et al. (1978) and Yagüe et al. (2001), the Beljaars and Holtslag (1991) relation, and the Zilitinkevich and Calanca (2000) model.

Note also that a plot of Ri versus ζ by definition is not affected by the self-correlation. For this reason, Fig. 7b is simply a plot of Ri versus z_n/L_n. The plots in Fig. 7 are an additional verification of the proposed SHEBA profile functions (9) (solid lines in the figure). The greater scatter of points in Fig. 7 for $\zeta < 0.05$ results from the relatively small sensible heat flux and unreliable temperature-gradient measurements in near-neutral conditions. The obtained asymptotic behaviours of $\varphi_m(\zeta)$ and $\varphi_h(\zeta)$ for $\zeta \to \infty$ imply that $\mathrm{Pr}_t \propto \zeta^{-1/3}$, $\mathrm{Ri} \propto \zeta^{1/3}$, and $\mathrm{Rf} \propto \zeta^{2/3}$ in the limit of very strong stability.

The integral form of $\varphi_{m\ \mathrm{SHEBA}}$ can be obtained by integrating Eq. 6a with $\varphi_m(\zeta)$ defined by Eq. 9a,

$$\begin{aligned}\Psi_{m\ \mathrm{SHEBA}}(\zeta) &= \int_0^{\zeta} \frac{1-\varphi_{m\ \mathrm{SHEBA}}(\xi)}{\xi}\mathrm{d}\xi \\ &= -\frac{3a_m}{b_m}(x-1) + \frac{a_m B_m}{2b_m}\left[2\ln\frac{x+B_m}{1+B_m} - \ln\frac{x^2 - xB_m + B_m^2}{1-B_m+B_m^2}\right. \\ &\quad \left. + 2\sqrt{3}\left(\arctan\frac{2x-B_m}{\sqrt{3}B_m} - \arctan\frac{2-B_m}{\sqrt{3}B_m}\right)\right], \end{aligned} \tag{12}$$

where $x = (1+\zeta)^{1/3}$, $B_m = \left(\frac{1-b_m}{b_m}\right)^{1/3} > 0$. In a similar way to Eq. 12, the integral form of the $\varphi_{h\ \mathrm{SHEBA}}$ can be obtained from Eqs. 6b, 9b:

$$\begin{aligned}\Psi_{h\ \mathrm{SHEBA}}(\zeta) &= \int_0^{\zeta} \frac{1-\varphi_{h\ \mathrm{SHEBA}}(\xi)}{\xi}\mathrm{d}\xi \\ &= -\frac{b_h}{2}\ln\left(1 + c_h\zeta + \zeta^2\right) + \left(-\frac{a_h}{B_h} + \frac{b_h c_h}{2B_h}\right) \\ &\quad \times \left(\ln\frac{2\zeta + c_h - B_h}{2\zeta + c_h + B_h} - \ln\frac{c_h - B_h}{c_h + B_h}\right), \end{aligned} \tag{13}$$

where $B_h = \sqrt{c_h^2 - 4} = \sqrt{5}$. Equations 12 and 13 are more complicated than the Kansas-type, the Beljaars–Holtslag, and Cheng–Brutsaert $\Psi_m(\zeta)$ and $\Psi_h(\zeta)$functions. However, Eqs. 12 and 13 are analytical relationships based on the $\varphi_m(\zeta)$ and $\varphi_h(\zeta)$ functions (9a) and (9b) that better fit the SHEBA data. Applying the functional forms (12) and (13) to wind speed (5a) and temperature (5b) profiles is straightforward. The proposed SHEBA profile functions (9) are valid for $\mathrm{Ri}_B < \mathrm{Ri}_{B\,cr} \approx 0.2$. The bulk Richardson number, Eq. 8, may be estimated from Eqs. 5, 12, and 13.

6 Conclusions

We have used the comprehensive SHEBA flux–profile data to understand the behaviour of the profile stability functions, φ_m and φ_h, and derive quantities such

as the turbulent Prandtl number, Pr_t, and the gradient Richardson number in the stably stratified atmospheric boundary layer.

According to the SHEBA data, both stability functions φ_m and φ_h increase more slowly in very stable conditions than predicted by the linear equations (4) and the Beljaars–Holtslag relationship. In the limit of very strong stability, φ_m varies as $\zeta^{1/3}$; whereas φ_h initially increases with increasing ζ, reaches a maximum at $\zeta \approx 10$, and then tends to level off with increasing ζ. The scaling law $\varphi_m \propto \zeta^{1/3}$ is associated with our proposed frictionless or 'u_*-less' scaling. As a consequence of the observed dependences for the stability functions φ_m and φ_h, the turbulent Prandtl number decreases and tends to be less than 1 ($\mathrm{Pr}_t \propto \zeta^{-1/3}$) with increasing stability. This result implies that heat transfer is more efficient than momentum transfer in the very stable regime.

Based on the SHEBA data, we propose new mathematical forms for φ_m and φ_h in stable conditions, Eq. 9. The SHEBA measurements also show that profile stability functions based on local scaling are more scattered than those based on surface scaling. We took special care when analyzing φ_m and φ_h as functions of ζ in light of the self-correlation problem. For independent estimates of how φ_m and φ_h behave in very stable stratification, we plotted these functions against the bulk Richardson number. In addition, to analyze φ_m and φ_h as functions of ζ, we used an independent bin-averaging method instead of conventional averaging.

Acknowledgements The U.S. National Science Foundation supported this work with awards to the NOAA Environmental Technology Laboratory (now Earth System Research Laboratory) (OPP-97-01766), the Cooperative Institute for Research in Environmental Sciences (CIRES), University of Colorado (OPP-00-84322, OPP-00-84323), the U.S. Army Cold Regions Research and Engineering Laboratory (OPP-97-02025, OPP-00-84190), and the Naval Postgraduate School (OPP-97-01390, OPP-00-84279). The U.S. Department of the Army also supported ELA through Project 611102T2400. Thanks go to Reg Hill and Bob Banta for suggestions on improving the manuscript. Comments from anonymous reviewers are greatly appreciated.

References

Andreas EL (2002) Parameterizing scalar transfer over snow and ice: a review. J Hydrometeorol 3:417–432

Andreas EL, Hicks BB (2002) Comments on critical test of the validity of Monin-Obukhov similarity during convective conditions. J Atmos Sci 59:2605–2607

Andreas EL, Fairall CW, Guest PS, Persson POG (1999) An overview of the SHEBA atmospheric surface flux program. 13th symposium on boundary layers and turbulence. Dallas, TX, Amer Meteorol Soc, Proceedings, pp 550–555

Andreas EL, Claffey KJ, Makshtas AP (2000) Low-level atmospheric jets and inversions over the Western Weddell Sea. Boundary-Layer Meteorol 97:459–486

Andreas EL, Claffey KJ, Jordan RE, Fairall CW, Guest PS, Persson POG, Grachev AA (2006) Evaluations of the von Kármán constant in the atmospheric surface layer. J Fluid Mech 559: 117–149

Andreas EL, Guest PS, Persson POG, Fairall CW, Horst TW, Moritz RE, Semmer SR (2002) Near-surface water vapor over sea ice is always near ice saturation. J Geophys Res 107(C10), doi: 10.1029/2000JC000411

Andreas EL, Fairall CW, Grachev AA, Guest PS, Horst TW, Jordan RE, Persson POG (2003) Turbulent transfer coefficients and roughness lengths over sea ice: the SHEBA results. In Seventh conference on polar meteorology and oceanography and joint symposium on high-latitude climate variations, American Meteorological Society. 12–16 May 2003, Hyannis, Massachusetts, AMS Preprint CD-ROM

Beljaars ACM, Holtslag AAM (1991) Flux parameterization over land surfaces for atmospheric models. J Appl Meteorol 30(3):327–341

Businger JA, Wyngaard JC, Izumi Y, Bradley EF (1971) Flux–profile relationships in the atmospheric surface layer. J Atmos Sci 28:181–189
Carl MD, Tarbell TC, Panofsky HA (1973) Profiles of wind and temperature from towers over homogeneous terrain. J Atmos Sci 30:788–794
Cheng Y, Brutsaert W (2005) Flux–profile relationships for wind speed and temperature in the stable atmospheric boundary layer. Boundary-Layer Meteorol 114(3):519–538
Clement RJ (2004) Mass and energy exchange of a plantation forest in Scotland using micrometeorological methods. PhD Thesis, The University of Edinburgh, School of Geosciences, 597 p. (http://www.geos.ed.ac.uk/homes/rclement/PHD/)
Dyer AJ (1974) A review of flux–profile relationships. Boundary-Layer Meteorol. 7:363–372
Dyer AJ, Bradley EF (1982) An alternative analysis of flux–gradient relationships at the 1976 ITCE. Boundary-Layer Meteorol 22:3–19
Dyer AJ, Hicks BB (1970) Flux–gradient relationships in the constant flux layer. Quart J Roy Meteorol Soc 96:715–721
Forrer J, Rotach MW (1997) On the turbulence structure in the stable boundary layer over the Greenland ice sheet. Boundary-Layer Meteorol 85:111–136
Garratt JR (1992) The atmospheric boundary layer. Cambridge University Press, Cambridge, 316 pp
Grachev AA, Fairall CW, Persson POG, Andreas EL, Guest PS (2002) Stable boundary-layer regimes observed during the SHEBA Experiment. In 15th symposium on boundary layers and turbulence. Wageningen, The Netherlands, Amer. Meteorol. Soc., Proc., 374 – 377
Grachev AA, Fairall CW, Persson POG, Andreas EL, Guest PS, Jordan RE (2003) Turbulence decay in the stable arctic boundary layer. In Seventh conference on polar meteorology and oceanography and joint symposium on high-latitude climate variations. Hyannis, Massachusetts, Amer. Meteorol. Soc., Preprint CD-ROM
Grachev AA, Fairall CW, Persson POG, Andreas EL, Guest PS (2005) Stable boundary-layer scaling regimes: The SHEBA data. Boundary-Layer Meteorol 116(2):201–235
Hartogensis OK, De Bruin HAR (2005) Monin–Obukhov similarity functions of the structure parameter of temperature and turbulent kinetic energy dissipation rate in the stable boundary layer. Boundary-Layer Meteorol 116(2):253–276
Hicks BB (1978) Comments on 'The characteristics of turbulent velocity components in the surface layer under convective conditions'. by H. A. Panofsky, et al. Boundary-Layer Meteorol. 15(2):255–258
Högström U (1988) Non-dimensional wind and temperature profiles in the atmospheric surface layer: a re-evaluation. Boundary-Layer Meteorol 42:55–78
Holtslag AAM, De Bruin HAR (1988) Applied modeling of the nighttime surface energy balance over land. J Appl Meteorol 27:689–704
Holtslag AAM, Nieuwstadt FTM (1986) Scaling the atmospheric boundary layer. Boundary-Layer Meteorol 36:201–209
Horst T (2000) On frequency response corrections for eddy covariance flux measurements. Boundary-Layer Meteorol 94(3):517–520
Howell JF, Sun J (1999) Surface-layer fluxes in stable conditions. Boundary-Layer Meteorol 90:495–520
Kader BA, Yaglom AM (1990) Mean fields and fluctuation moments in unstably stratified turbulent boundary layers. J Fluid Mech 212:637–662
Kaimal JC, Finnigan JJ (1994) Atmospheric boundary layer flows: their structure and measurements. Oxford University Press, New York, Oxford, 289 pp
King JC (1990) Some measurements of turbulence over an Antarctic shelf. Quart J Roy Meteorol Soc 116:379–400
Klipp CL, Mahrt L (2004) Flux–gradient relationship, self-correlation and intermittency in the stable boundary layer. Quart J Roy Meteorol Soc 130(601):2087–2103
Kondo J, Kanechika O, Yasuda N (1978) Heat and momentum transfers under strong stability in the atmospheric surface layer. J Atmos Sci 35:1012–1021
Kristensen L, Fitzjarrald DR (1984) The effect of line averaging on scalar flux measurements with a sonic anemometer near the surface. J Atmos Oceanic Technol 1(3):138–146
Mahrt L (1999) Stratified atmospheric boundary layers. Boundary-Layer Meteorol 90:375–396
Mahrt L, Vickers D (2002) Contrasting vertical structures of nocturnal boundary layers. Boundary-Layer Meteorol 105:351–363
Mahrt L, Sun J, Blumen W, Delany T, Oncley S (1998) Nocturnal boundary-layer regimes. Boundary-Layer Meteorol 88:255–278

Massman WJ (2000) A simple method for estimating frequency response corrections for eddy covariance systems. Agric Forest Meteorol 104:185–198
Monin AS, Obukhov AM (1954) Basic laws of turbulent mixing in the surface layer of the atmosphere. Trudy Geofiz Inst Acad Nauk SSSR 24:163–187
Monin AS, Yaglom AM (1971) Statistical fluid mechanics: mechanics of turbulence, vol 1. MIT Press, Cambridge, Massachusetts, 769 pp
Moore CJ (1986) Frequency response corrections for eddy correlation systems. Boundary-Layer Meteorol 37(1–2):17–36
Nieuwstadt FTM (1984) The turbulent structure of the stable, nocturnal boundary layer. J Atmos Sci 41:2202–2216
Obukhov AM (1946) Turbulence in an atmosphere with a non-uniform temperature. Trudy Inst Teoret Geofiz Akad Nauk SSSR 1:95–115
Obukhov AM (1971) Turbulence in an atmosphere with a non-uniform temperature. Boundary-Layer Meteorol 2:2–29
Panofsky HA (1963) Determination of stress from wind and temperature measurements. Quart J Roy Meteorol Soc 89:85–94
Pahlow M, Parlange MB, Porté-Agel F (2001) On Monin–Obukhov similarity in the stable atmospheric boundary layer. Boundary-Layer Meteorol. 99:225–248
Paulson CA (1970) The mathematical representation of wind speed and temperature profiles in the unstable atmospheric surface layer. J Appl Meteorol 9:857–861
Paw UKT, Baldocchi DD, Meyers TP, Wilson KB (2000) Correction of eddy-covariance measurements incorporating both advective effects and density fluxes. Boundary-Layer Meteorol 97(3):487–511
Persson POG, Fairall CW, Andreas EL, Guest PS, Perovich DK (2002) Measurements near the atmospheric surface flux group tower at SHEBA: near-surface conditions and surface energy budget. J Geophys Res 107(C10):8045, doi: 10.1029/2000JC000705
Smedman A-S (1988) Observations of a multi-level turbulence structure in a very stable atmospheric boundary layer. Boundary-Layer Meteorol 44:231–253
Sorbjan Z (1989) Structure of the atmospheric boundary layer. Prentice-Hall, New Jersey, 317 pp
Uttal T, 27 co-authors (2002) Surface heat budget of the Arctic ocean. Bull Am Meteorol Soc 83:255–276
Webb EK (1970) Profile relationships: the log-linear range, and extension to strong stability. Quart J Roy Meteorol Soc 96:67–90
Wilczak JM, Oncley SP, Stage SA (2001) Sonic anemometer tilt correction algorithms. Boundary-Layer Meteorol 99(1):127–150
Wilson DK (2001) An alternative function for the wind and temperature gradients in unstable surface layers. Boundary-Layer Meteorol 99:151–158
Wyngaard JC (1973) On surface-layer turbulence. In Haugen DA (ed) Workshop on micrometeorology. American Meteorology Society, Boston, Mass, pp 101–149
Wyngaard JC, Coté OR (1972) Cospectral similarity in the atmospheric surface layer. Quart J Roy Meteorol Soc 98:590–603
Yaglom AM (1977) Comments on wind and temperature flux–profile relationships. Boundary-Layer Meteorol 11:89–102
Yagüe C, Maqueda G, Rees JM (2001) Characteristics of turbulence in the lower atmosphere at Halley IV Station, Antarctica. Dyn Atmos Ocean 34:205–223
Yagüe C, Viana S, Maqueda G, Redondo JM (2006) Influence of stability on the flux–profile relationships for wind speed, φ_m, and temperature, φ_h, for the stable atmospheric boundary layer. Nonlin Processes Geophys 13(2):185–203
Zilitinkevich S, Baklanov A (2002) Calculation of the height of the stable boundary layer in practical applications. Boundary-Layer Meteorol 105:389–409
Zilitinkevich S, Calanca P (2000) An extended similarity-theory for the stably stratified atmospheric surface layer. Quart J Roy Meteorol Soc 126:1913–1923
Zilitinkevich SS, Chalikov DV (1968) Determining the universal wind-velocity and temperature profiles in the atmospheric boundary layer. Izvestiya Acad Sci USSR Atmos Oceanic Phys 4:165–170 (English Edition)
Zilitinkevich S, Mironov DV (1996) A multi-limit formulation for the equilibrium depth of a stably stratified boundary layer. Boundary-Layer Meteorol 81:325–351